29th AIAA Applied Aerodynamics Conference
27 - 30 June 2011, Honolulu, Hawaii

AIAA 2011-3357

Some Effects of Blowing, Suction and Trailing Edge Bluntness on Flow Separation from Thick Airfoils; Computations & Measurements

Roman Seele[1]
California Institute of Technology, Pasadena, California, 91125, USA

Chunmei Chen[2], Cristina Bhamburkar[3], and Israel Wygnanski[4]
The University of Arizona, Tucson, Arizona 85721, USA

The relative effectiveness of blowing and suction in controlling separation and circulation is assessed in the present paper. This paper focuses on low momentum input from the leading and trailing edge regions and the effects of a sharp and round trailing edges. Blowing is most effective when it is applied near but upstream of the separation location for the narrowest slot possible. The effectiveness of suction improves when the slot is located near but downstream of the natural separation location and it is as wide as possible. The effects of adding different trailing edge shapes on separation control were also explored. Most of the data presented was taken at incompressible speeds and at Re < 2.5*10^5.

NOMENCLATURE

C = chord length
C_D = drag coefficient: $D / q\, c$
C_L = lift coefficient: $L / q\, c$
C_P = pressure coefficient: $(p - p_\infty) / q$
C_Q = steady volume flow coefficient: Q / cU_∞
CW = Slot is oriented in clockwise direction
C_μ = steady momentum coefficient: $(2h/C)(U_{Slot}/U_\infty)^2 = 2C_Q(U_{Slot}/U_\infty)$
D = drag
h = slot width
L = lift
LE = leading edge
q = dynamic pressure: $\rho U_\infty^2 / 2$
Q = volume flow through the slot
R = radius of the trailing and leading edges of the airfoil investigated
Re = Reynolds Number: $U_\infty c / \nu$
TE = trailing edge
U_j = slot velocity assumed to be "top-hat"
U_∞ = free stream velocity
x_c = distance from slot to trailing edge
α = angle of attack
δ_f = flap deflection
θ = angular distance measured from the chord line near the TE or LE of a circular cylinder

[1] Research Associate, Graduate Aerospace Laboratories.
[2] Post Doctoral Scholar, Department of Aerospace and Mechanical Engineering.
[3] Research Assistant, Department of Aerospace and Mechanical Engineering.
[4] Professor, Department of Aerospace and Mechanical Engineering, AIAA Fellow.

I. BACKGROUND

Flow separation represents the detachment of fluid from a solid surface (e.g. Maskell, [1]; Chang [2]; Telionis [3]; Gad-el-Hak & Bushnell [4]). It is accompanied by significant thickening of the rotational flow adjacent to the surface and a marked increase in the velocity component normal to it. Whatever the cause of separation may be (severe adverse pressure gradient e.g. Simpson [5] and [6], large curvature, or a geometrical aberration e.g. Bradshaw & Wong [7]; Kim [8]), the boundary layer approximation is invalidated. Separation is always associated with a loss of lift and an increase in drag, consequently many attempts of delaying it, altering its location, or avoiding it altogether were made. The shapes of streamlined configurations used in aeronautics bear testimony to the efforts made in avoiding separation.

Prandtl [9] demonstrated that flow separation from the surface of a circular cylinder can be substantially delayed by sucking the boundary layer through a narrow slot. However, as the quest for speed increased, and the wing sections became thinner, suction gave way to blowing of high pressure air that could be conveyed in small diameter pipes. Jet propulsion that availed relatively large quantities of compressed air onto airborne systems enabled blowing to become the standard technique used for lift augmentation. Massive blowing that increased the lift above and beyond the nominal values provided by conventional control surfaces, created a device known as "jet-flap", or as it is more recently referred to, circulation control. Nevertheless, boundary layer control by blowing was used sparsely, even on military airplanes, because of the substantial power required for its application and the added complexity and weight of its installation.

II. EXPERIMENTAL APPARATUS

A. Geometry

The basic elliptical airfoil (Fig. 1) has a chord of 10.86" and a maximum thickness to chord ratio of 30%. The circular arcs that form its leading and trailing edges are 2.46" in diameter and they fit snuggly into the main body of the airfoil. The slots are inclined at 30^{o} to the surface and their width and location can be adjusted in situ by rotating the individual arcs and placing the appropriate spacers into the slots before tightening the end plates. The symmetry of the configuration enables tests at positive and negative incidence angles thus changing the surface (lower or upper) from which the jet emanates. Rotation of the slot orientation or change in the slot location provides added flexibility that might affect the leading edge stall angle and the behavior of the airfoil near stall. An "I" beam divides the interior volume of the airfoil into two independent pressure chambers through which compressed air can be passed either independently or in conjunction with the other slot and chamber.

.

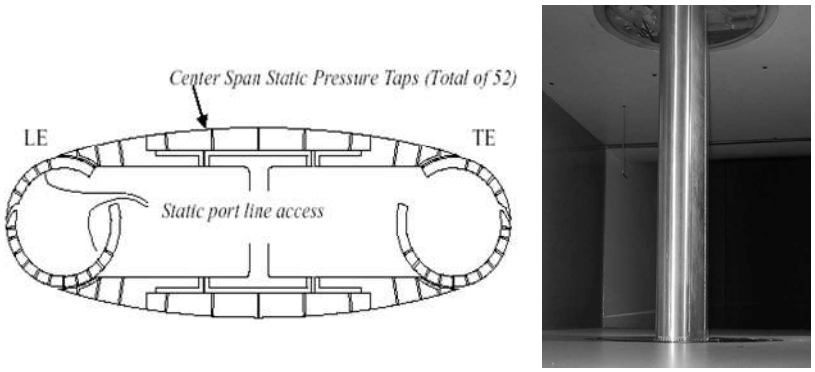

Fig. 1 A cross section of the elliptical airfoil without cusp and a picture of its installation in the wind tunnel

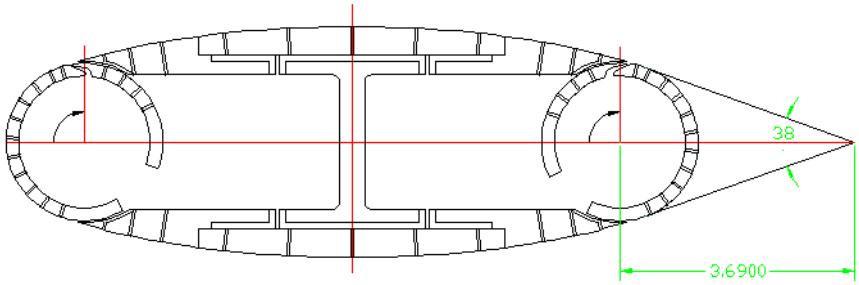

Fig. 2 Diagram of the Ellipse with the Cusp Attachment

B. Experimental Measurements

The airfoil is equipped with 52 static pressure taps (Fig. 1) from which the lift and the form-drag component were calculated. Total drag was measured by traversing the wake some 3 chord lengths downstream of the trailing edge where the static pressure corrections were small. The wake rake consisted of 15 total-pressure probes that were placed at an interval of 1" and two static pressure probes located at both ends of the rake. The rake could slide relative to the airfoil and could thus be centered in the airfoil's wake. It could also be traversed across the wake in order to provide the necessary resolution of data points wherever the velocity gradients were steep. All pressure ports were scanned electronically using Pressure Systems Inc. (PSI) modules. These modules have an array of silicon piezo-resistive pressure sensors, one for each pressure port. The sensors are calibrated by connecting them to a common manifold of known pressure through two-position pneumatically actuated valves.

A hot wire anemometer was used to calibrate the slot whenever the actuation method demanded it. The constant temperature anemometer (AA systems model AN 1003) was used in conjunction with a single wire probe that was inserted into the slot. The wire was calibrated in the free stream and the flow through the slot was assumed to be uniform across it.

The 24" span model was installed in a 24-inch by 41-inch test section of an open loop, cascade wind tunnel. The Reynolds numbers tested varied between 100,000 and 500,000. In order to avoid laminar bubbles and strong Reynolds number dependence, four roughness strips were used on both surfaces of the elliptical airfoil: two were placed at mid chord and two at the juncture between the LE cylinder and the main element. This insured that the flow was turbulent upstream of the controlled separation. The installation of the airfoil in the tunnel is shown in Fig. 1.

A small blower could provide up to 68 SCFM at a maximum pressure of 800mm of water. The air supplied passed through a flow meter of the appropriate range. The input voltage regulated the RPM of the blower and thus the volume flow through the slot. The air leaving the flow meter outlet passed through two flexible hoses connected to both sides of a settling chamber in the interior of the airfoil, thus maximizing the contraction ratio between the inlet and the slot areas.

Particle Image Velocimetry (PIV) was used to explain some observations made. The system consists of one Kodak Megaplus CCD camera with a resolution of 1008*x*1018 pixels, a Nd:YAG laser, standard light sheet forming optics, a synchronization and timing unit to control the laser and camera timing and a commercially available PIV evaluation software (IDT proVISION-XS). The light sheet enters through the side into the wind tunnel. For calibration purposes, the camera is focused on a target that is mounted in the wind tunnel near the airfoil and aligned with the laser light sheet. 250 snapshots were taken at each location for a desired flow condition. This number sufficed as the data was only used to describe the flow field qualitatively.

C. Grid Generation

Using the Overgrid graphical user interface, a C-grid was built with dimensions 529 streamwise x 97 normal x 2 span-wise (Fig. 3). There are 91 streamwise points in the wake, which extends a distance 20 times the chord length. The grid is split in the streamwise direction into 8 grid blocks to allow for computation in parallel mode. The individual grid blocks have dimensions 67x97x2. Although the case is 2D, CFL3D is a finite volume code requiring a 3D grid, so 2 grid points must be defined in the span-wise direction. Outside the grid in the span-wise direction, a boundary condition is set up to extrapolate ghost points outside the flowfield domain (Fig. 3).

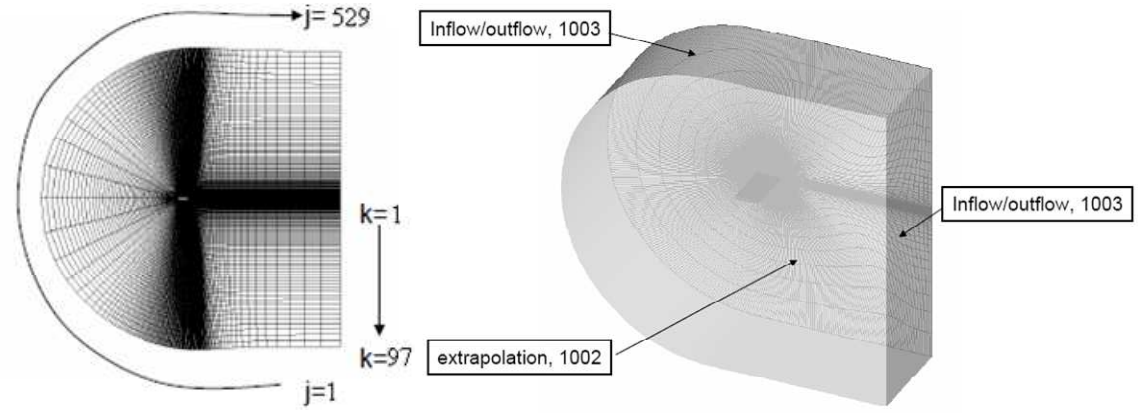

Fig. 3 Outer boundary conditions for a C-grid

D. CFD Software CFL3D

Results are computed using CFL3D Version 6.4, a Reynolds-averaged thin-layer Navier-Stokes computational fluid dynamics code for structured grids. The spatial discretization uses a finite-volume approach. The implicit time advancement can solve steady and unsteady flows. Weiss-Smith low Mach number preconditioning is also implemented. The code is parallelized with Message Passing Interface (MPI) protocol. Also, the code offers numerous turbulence models. Four models have been tested, including Baldwin-Lomax, Spalart-Allmaras, Wilcox k-omega, and Menter SST k-omega. For all the cases under consideration, the Mach number was approximately 0.05 and the Reynolds number was 300,000.

III. RESULTS AND DISCUSSION

E. Baseline Flow

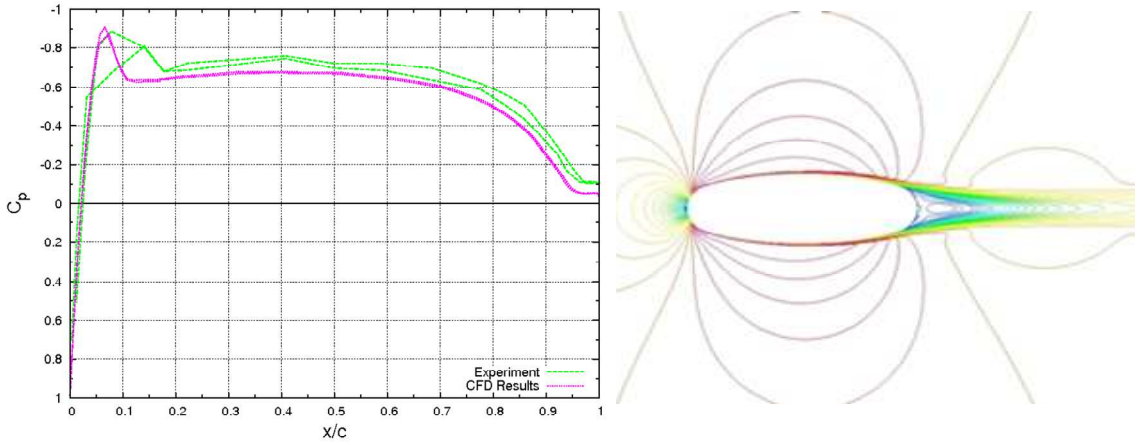

Fig. 4 Computed C_p on the ellipse and velocity contours around it at zero angle of attack

Fig. 4a shows the pressure coefficient on the surface of the ellipse computed by using CFL3D at zero angle of attack. It is plotted alongside experimental results obtained from the wind tunnel at the University of Arizona's Aerodynamics Laboratory. From the figure it is clear that the predicted pressure coefficient is similar to the experimentally obtained pressure coefficient, especially at the trailing edge where the flow is separated and the pressure coefficient reaches a low negative constant value. The main differences are that the CFD results slightly underestimate the value of the pressure coefficient across much of the surface. Also, CFD results predict a greater

spike in the pressure coefficient near the leading edge than in the experimental results, which predict smoother values of the pressure coefficient near the leading edge.

Fig. 4b shows the velocity contours for the ellipse at α=0°. The contour lines represent lines of constant velocity magnitude, where the red lines represent high velocity, while the blue lines indicate a low (near zero) velocity. Low velocities appear at the stagnation point at the leading edge, and in the wake close to the body. High velocities are most prevalent along the upper surface at incidence in particular near the leading edge of the ellipse.

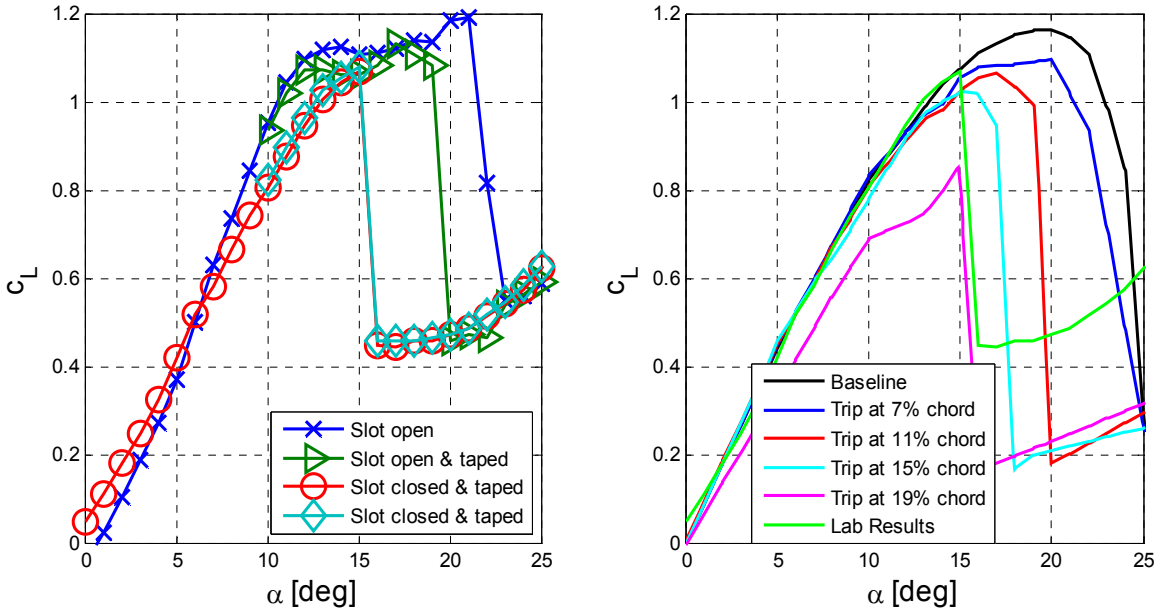

Fig. 5 C_L vs. α measured (a) at Re=250,000 and computed (b) using the Spalart-Allmaras Model (baseline is fully turbulent)

F. Lift generation-Effect of Tripping on Computation and Experiment

Before discussing the effects that flow control may have on the delay of separation it is important to document the baseline flow conditions prior to stall or immediately after its occurrence as a result of excessive incidence. The existence of an open slot affects the maximum lift generated by the airfoil because of surface discontinuity and possibly because the cavity in the interior of the airfoil resonates with various instability modes that may trip the laminar boundary layer. This is particularly significant at Reynolds numbers that are close to the naturally occurring transition near the leading edge because the tripping devices are located on the main element downstream of the cylindrical leading edge. An example for such sensitivity is shown in Fig. 5 where the slot, oriented in the direction of streaming, is located at an azimuth of 30° relative to the LE of the airfoil. Keeping the slot open and increasing the incidence angle generates a maximum lift coefficient of $C_{Lmax.}$=1.2. This also results in a gentle stall having $dC_L/d\alpha \approx 0$ over a wide range of incidence angles ($12^o < \alpha < 20^o$). The airfoil stalls at α=22° with a concomitant decrease in C_L of 50%. Taping over the open slot lowers the incidence at which the airfoil stalls without affecting C_{Lmax} in a substantial manner. It is clear that the open slot generates perturbations that keep the flow attached. The tape over an open slot acts as a membrane that transmits pressure fluctuations between the boundary layer and the interior of the airfoil. For this reason the airfoil with the taped over slot stalls at α=19°, while the same airfoil with the slot closed stalls at α=15°. A trip strip is simulated by defining arbitrarily a laminar region at the leading edge of the airfoil. The leading edge was forced to maintain a laminar boundary layer up to 7%, 11%, 15%, and 19% of the chord length. In the experiments, the ellipse had a trip strip at 11% chord and transition occurred farther downstream of it. Fig. 5 shows plots of C_L vs. α for varying angles of attack for the ellipse with varying trip locations.

Fig. 5b shows that as the transition location is moved downstream, the angle of attack at which stall occurs is decreased as is $C_{Lmax.}$. This earlier stall agrees well with the actual behavior of the ellipse in the laboratory (Fig. 5a). It can be concluded that the fully turbulent baseline solution is not necessarily the one that compares best with experiment, and that the results are better when a realistic laminar-turbulent transition location is applied. From Fig.

5a it is clear that closing the LE slot pushes the transition location to some 15% chord generating $C_{Lmax.}$=1 and reducing α_{stall} to 15° while keeping the slot open trips the flow very close to the LE and generates $C_{Lmax.}$=1.2.

The Spalart –Allmaras model under-predicts the drag generated in the experiment by a factor of 2 at small angles of incidence when the flow separates from the aft body only (C_D predicted is 0.042 while $C_{Dmeasured}$=0.088; not shown). This shortcoming of the model is well known [10] whenever small zones of separated flow occur on wings. Although the extend of the separated zone is predicted correctly (Fig. 4) the mean pressure in it does not agree with experiment and contributes substantially to the discrepancies in the predicted drag. The prediction is much better when the flow over the entire upper surface had separated (i.e. post stall condition when C_D>0.16).

G. Trailing Edge Cusp

The sole difference between the elliptical cylinder and a thick symmetrical airfoil (strut) is the lack of defined Kutta condition at the trailing edge. In that respect the ellipse is similar to the circulation controlled airfoils investigated by Englar [11] that use the "Coanda Effect" to generate the excess circulation. The pressure distributions over the ellipse and the strut at incidence are similar, but fixing the Kutta condition has consequences. For controlling the separation near the trailing edge we shall follow the path established by Poisson-Quinton[12] by keeping α=0°, while changing the other parameters affecting the flow. The significance of slot location was examined but it will not be discussed presently because the focus is on comparison to CFD at one location given by θ=90° as shown in Fig. 2.

The triangular cusp added at the trailing edge of this airfoil enforces the Kutta condition and drastically changes the behavior of the airfoil. The length of the triangular attachment is approximately 3.69" and the two sides of the triangle enclose a blunt 38° angle. A diagram of this attachment to the ellipse is shown in Fig. 2.

The measured and calculated pressure coefficients on the surface of this "new" airfoil at α=0° are compared in Fig. 6. The shape of the Cp curve is very different from the one shown in Fig. 4 over the aft 50% of the chord. The flow is not as badly separated near the TE and (Cp)TE has a positive value of 0.2 instead of (Cp)TE=-0.1 for the blunt trailing edge (Fig. 4). Furthermore, there is an agreement between experiment and computation that results in an acceptable prediction of the total drag. The slight differences between the pressures on the lower and upper surfaces stem from different transition locations that were forced experimentally and computationally. PIV measurements (Fig. 6b) further indicate that the flow is not fully attached. This was not initially identified in the pressure distribution. Fig. 6b shows contours of the x-component of the velocity over the upper surface only because the lower surface was in the shade of the laser sheet. The white zone over the top surface marks stagnant air and it diverges with increasing distance toward the TE.

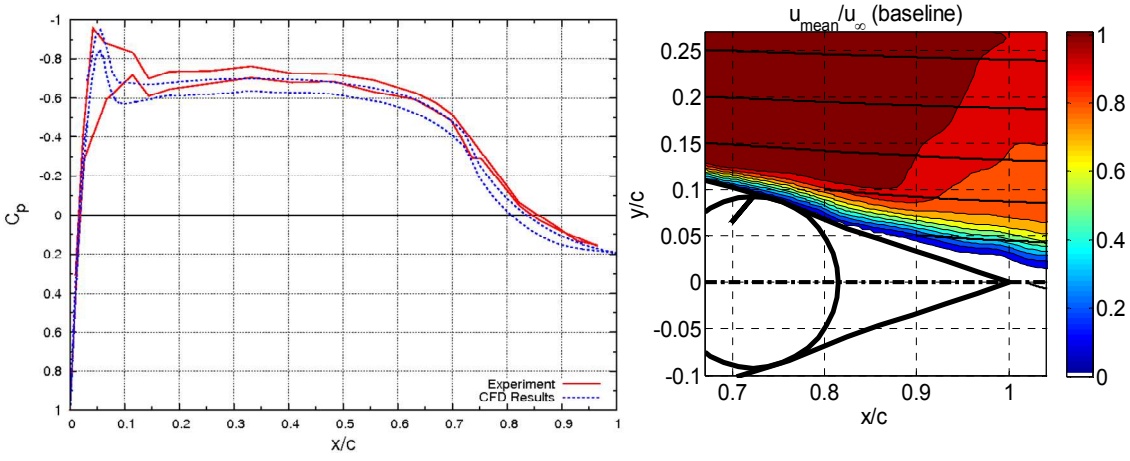

Fig. 6 C_p vs. x/c for the ellipse with a cusp at zero angle of attack

The effect of varying α on the lift generated by the cusped airfoil was considered next (**Fig. 7**). The cusp generates a deleterious effect on the lift at small angles of attack, which can be attributed to the large thickness ratio of the airfoil and the wide trailing edge wedge-angle. As α is increased, the separation zone increases above the upper loft, while the flow becomes entirely attached to the lower surface. This generates two effects near the TE:

(1) The flow downstream of the TE is inclined upward suggesting that an upward momentum is imparted to the fluid leaving the airfoil. This change in Y-component of momentum implies that a downward (negative) lift is generated.
(2) The curvature of the streamlines above the wedge suggest that the pressure above its upper surface should be higher than over its lower surface (See also Fig. 8) and that increase in pressure overpowers the lower pressure generated near the leading edge due to the positive incidence.

This negative lift effect cannot observed for the elliptical, blunt airfoil configuration, because the blunt TE does not shift the attachment and separation regions substantially enough to overcome the suction that is created at the LE due to an increase in α. Fig. 8b indicates that negative lift for the cusped airfoil occurs when the area under the curve of ΔC_P near the trailing edge surpasses the area under the curve near the leading edge. Both plots illustrate that CFD is able to predict the behavior that has been experienced in the laboratory.

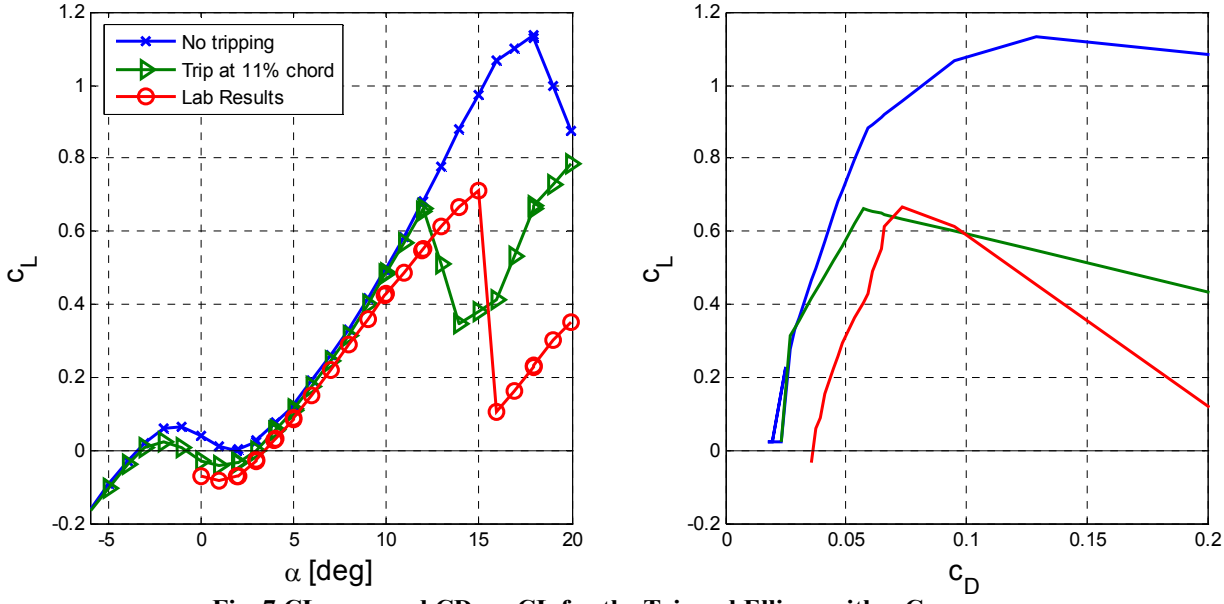

Fig. 7 CL vs. α and CD vs. CL for the Tripped Ellipse with a Cusp

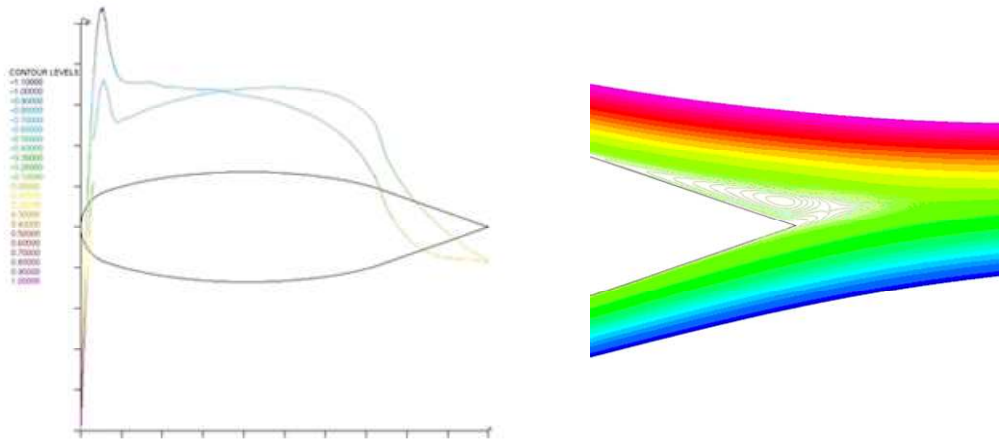

Fig. 8 Streamlines at the Trailing Edge of the cusped airfoil & the C_p distribution over its surface at α= 2°

Tripping at the leading edge may cause an earlier stall of the airfoil (**Fig. 7**), but does little to affect the negative lift-slope curve for small angles of attack. Comparing both CFD results with the lab tests shows that it is preferable to prescribe a laminar-turbulent transition location because it is predicts the stall angle of the airfoil better. Here, the transition location was prescribed at 11% of the chord, and so the predicted stall angle does not coincide with the lab results. Better results can be found by adjusting the trip location but this procedure was not warranted. The chosen

tripping location predicts the drag coefficient up to stall only reasonably well, underestimating the experimental drag data by some 30%.

H. Active Flow Control at the Trailing Edge

The experiment compares blowing to suction and focuses on relatively low momentum inputs. Slot location, and slot width were changed for each of the AFC methods used. In each application the input momentum and mass flow was altered. We shall focus on the comparison of steady blowing and suction by comparing both under identical flow conditions and on the ability of CFD to predict the results. Due to time and space limitations, the data presented in this paper represents only a small fraction of the data obtained throughout this investigation.

It was demonstrated before that blowing is most effective when it emanates from the narrowest slot possible at a given C_μ input while suction generates higher lift when the slot is widest [13, 14]. A comparison between suction and blowing at the narrowest slot width (where suction was least effective) and the widest slot width (where blowing was least effective) is shown in Fig. 9. At low values of C_μ suction is always beneficial while blowing is often detrimental. Even for the narrowest slot width, where suction is least effective the cross over between these two techniques occurs around $C_\mu = 0.9\%$. For the widest slot width blowing does not generate for $C_\mu<1.2\%$ while suction generates substantial lift ($C_L \approx 0.4$). Nevertheless, for high values of $C_\mu > 5\%$ blowing is still superior provided that the slot width is narrow and the trailing edge of the airfoil is blunt (circular or otherwise curved).

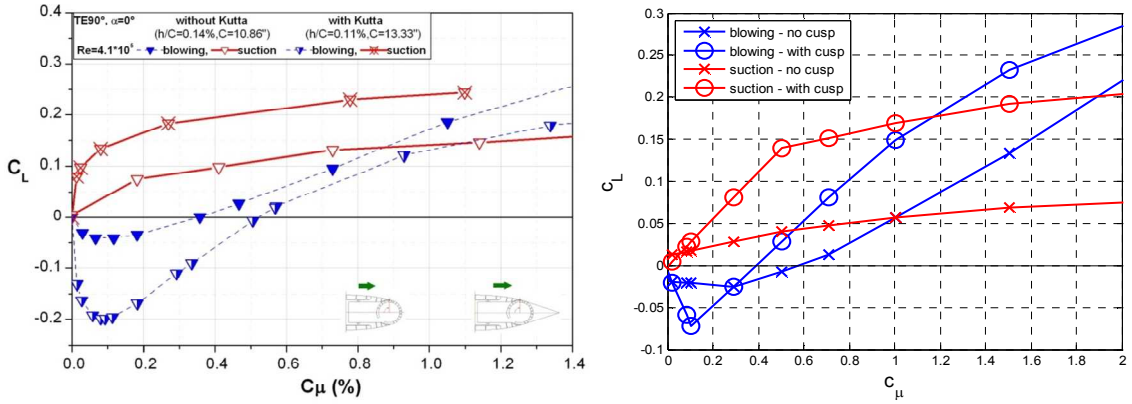

Fig. 9 The effect of a sharp trailing edge on the C_L that was generated by suction or blowing at low C_μ using the narrowest slot for measurements (left) and calculation (right)

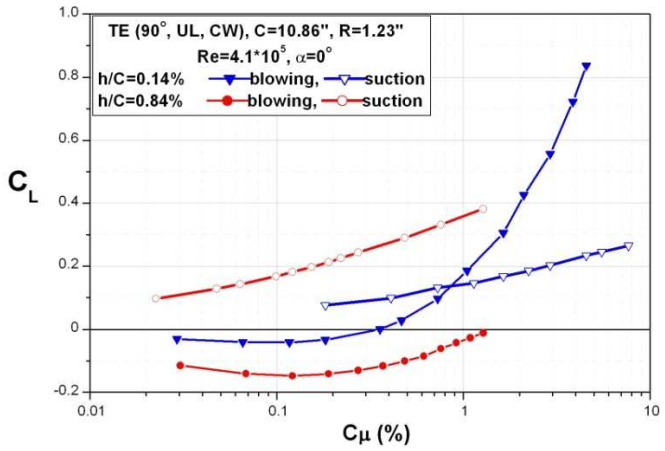

Fig. 10 The effect of the slot width on the C_L generated by suction or blowing at low levels of C_μ at Re=4.1*10^5

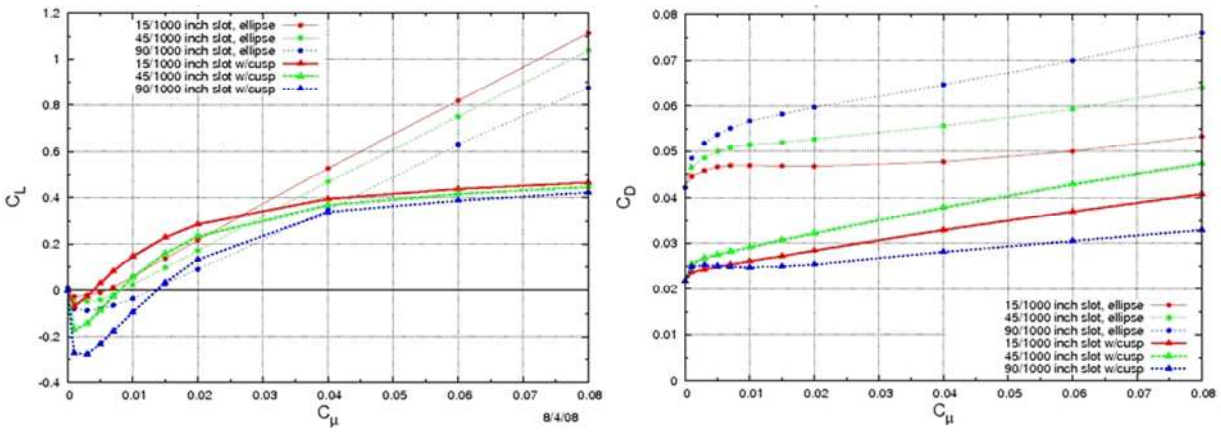

Fig. 11 C_L and C_D for blowing downstream for varying slot widths and C_μ (calculation)

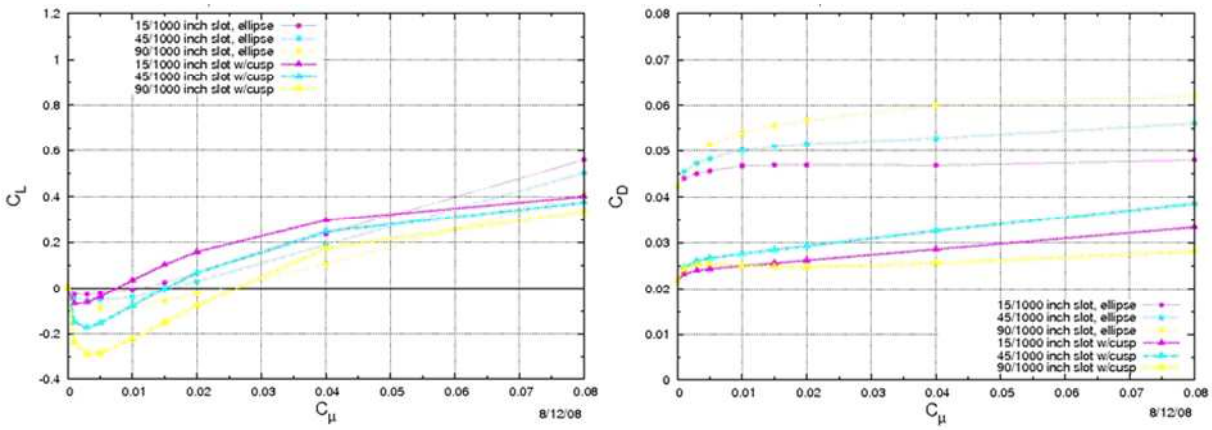

Fig. 12 C_L and C_D for suction upstream for varying slot widths and C_μ (calculation)

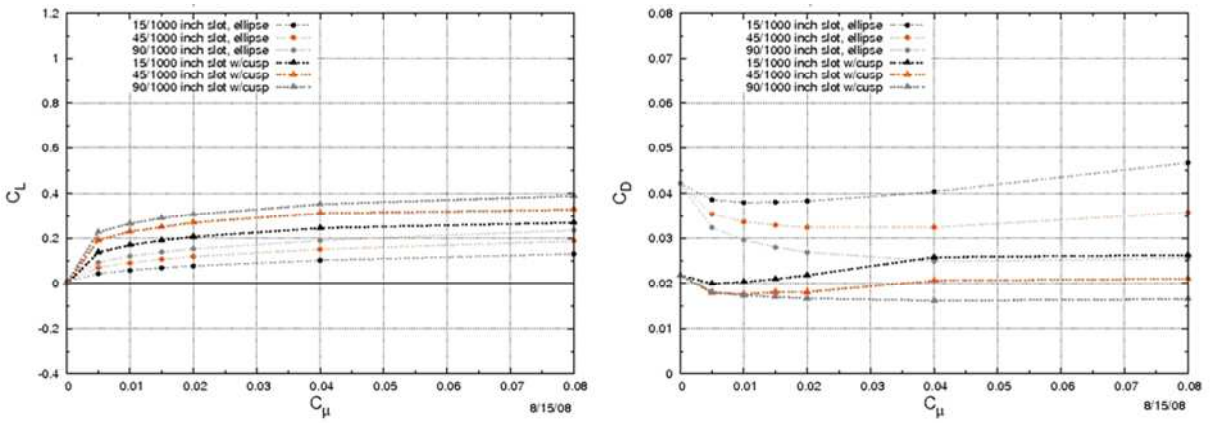

Fig. 13 C_L and C_D for suction downstream for varying slot widths and C_μ (calculation)

A sharp trailing edge that is not inclined relative to the chord line increases the lift generated by suction while decreasing it whenever blowing is used (Fig. 10). The sharp trailing edge prohibits the movement of the rear "stagnation" location to the lower surface at high values of C_μ (i.e. it does not allow changing Kutta condition due to blowing) but increases the entrainment from the lower-loft boundary layer downstream of the TE, which aggravates the deleterious effect of blowing. On the other hand, when suction is used in conjunction with a sharp TE, the flow from the lower loft is prevented from flowing into the slot, due to the sharp turning angle that the flow has to

overcome at the TE. Consequently, the sharp TE increases the upstream effect of suction and improves the generation of lift.

Next, suction and blowing were applied at the trailing edge of the ellipse with the slot pointing downstream in both cases. The slot width was varied from 15/1000 in. to 90/1000 in. and the value of the momentum coefficient was varied between 0% and 8%. All calculations were done at zero angle of attack. Plots were made of C_L vs. C_μ and C_D vs. C_μ to study how suction and blowing can best be utilized in active flow control. Fig. 11, Fig. 12 and Fig. 13 show plots of C_L vs. C_μ and C_D vs. C_μ with varying slot widths for both the ellipse and the ellipse with a cusp. Fig. 14 compares methods suction and blowing for a single value of the slot width. Fig. 15 compares one of these results to the results obtained experimentally for the ellipse with the cusp. From this figure, it is clear that CFD predicts the same negative lift for small values of the momentum coefficient. However, the values of the lift coefficient found in the lab are considerably lower than those predicted by CFD for high momentum coefficients. The lift coefficients predicted for suction are actually closer to the lab results for steady blowing for high momentum coefficients.

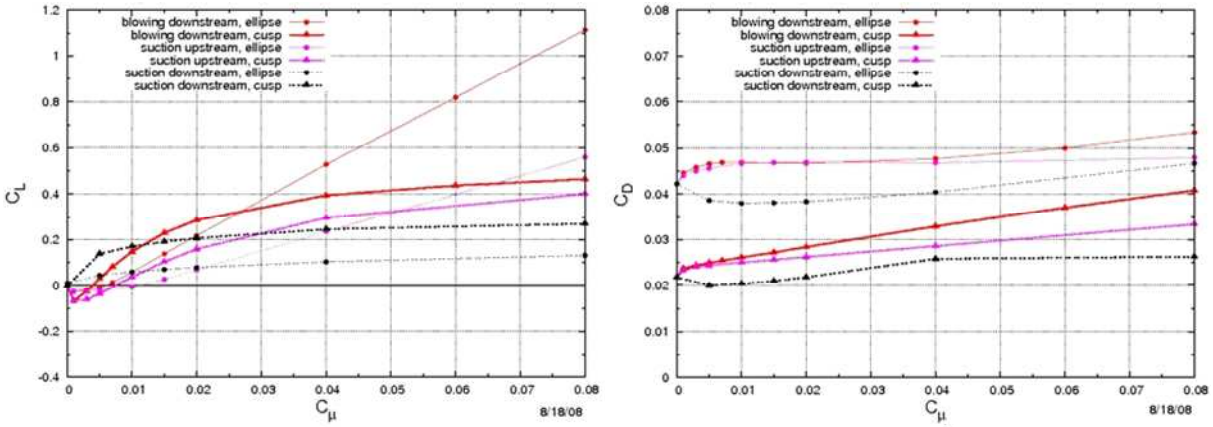

Fig. 14 C_L vs. C_μ and C_D vs. C_μ for TE suction and blowing at h = 0.015in. (calculation)

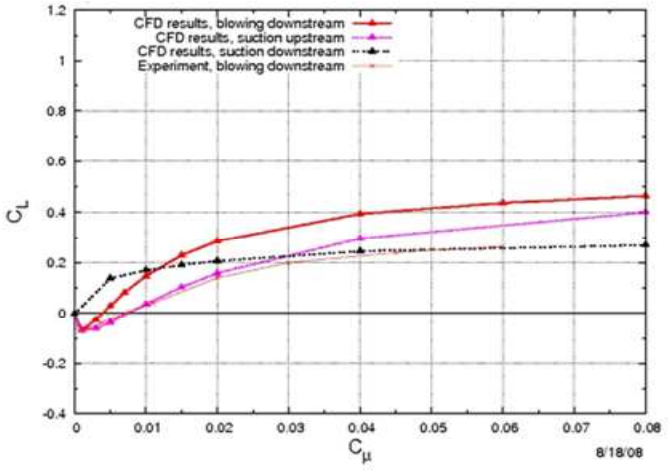

Fig. 15 C_L vs. C_μ for the Ellipse with Cusp, CFD and Lab Results, h=0.015in. (calculation)

Fig. 16 shows the velocity contours behind the ellipse when steady blowing is applied at C_μ = 8% without a cusp. This figure shows how blowing at high momentum coefficients alters the behavior near the trailing edge and results in very high lift coefficients even at zero angle of attack. Attaching the cusp to the TE results in negative lift. Stream Functions and PIV behind the airfoil (Fig. 17) both show this behavior. It is very similar to the stream function shown in Fig. 8 for the ellipse with a cusp at low angles of attack. Hence, it is concluded that the negative lift slope for low momentum coefficients occurs for a similar reason as it did for low angles of attack namely that it is a result of the high thickness of the airfoil coupled with a relatively high trailing edge cusp angle.

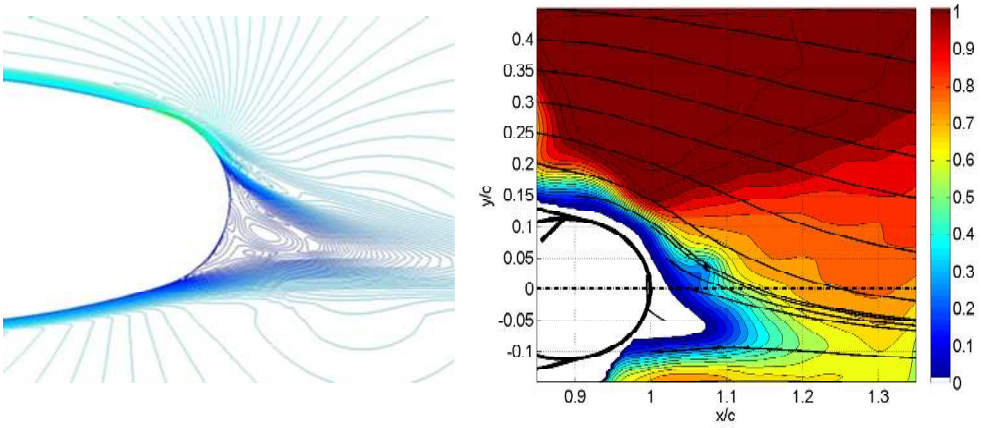

Fig. 16 Velocity contours for the ellipse with steady blowing, left: C_μ = 8% (calculation), right: C_μ = 10% (measurement)

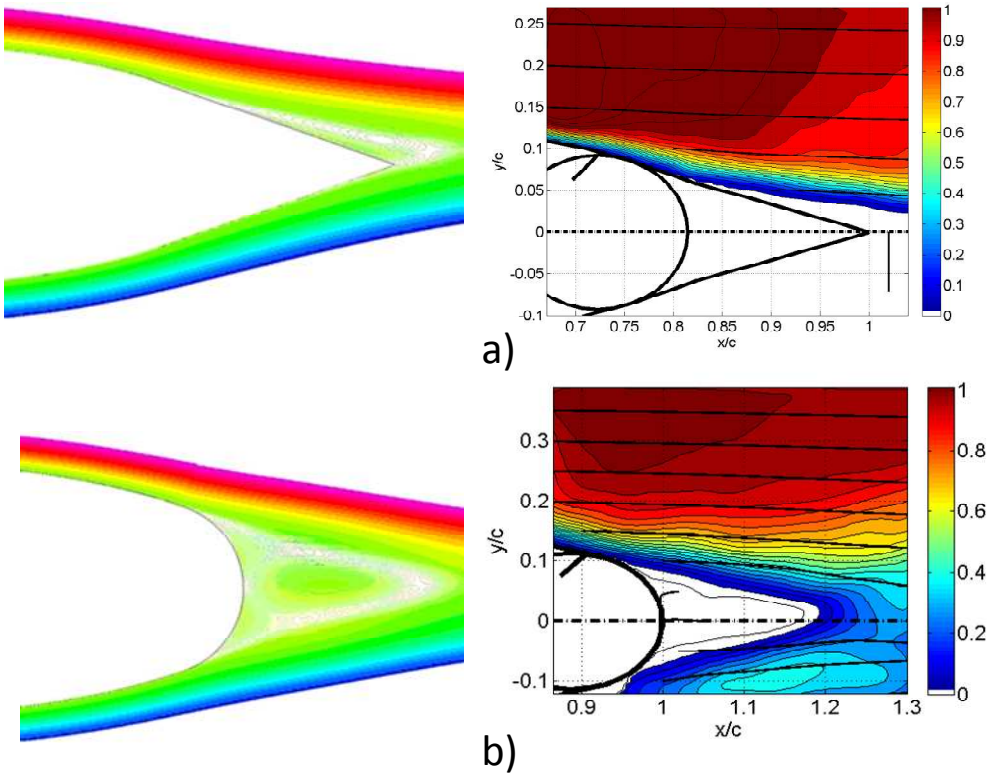

Fig. 17 Stream function for Blowing at C_μ = 0.1% and h=0.09" a) with cusp and b) without cusp

I. Steady Blowing Results from the Leading Edge Region

The use of flow control near the leading edge of an airfoil is mostly intended to delay separation at high values of C_L (mostly at high incidence) and ameliorate the adverse effects of stall. For steeply descending uninhabited aerial vehicles, one may be interested in destroying the lift and increasing the drag. This can be achieved by redirecting the blowing against the oncoming stream which is a very useful procedure provided that it is easily controllable. Since the mere existence of an open slot at $\theta=30^o$ from the LE affects the stalling characteristics of this airfoil, the effects of blowing are always compared to the corresponding baseline data obtained under identical test

conditions that include tripping devices and Re.

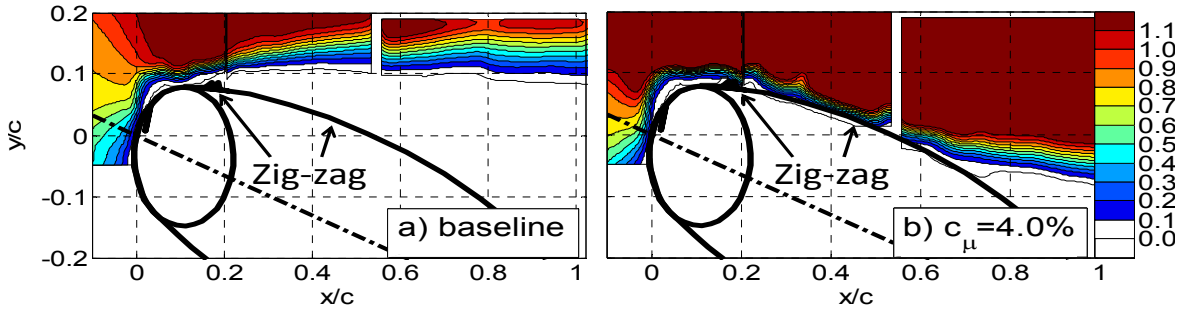

Fig. 18 Mean velocity contours over the upper surface of the Ellipse. Slot located on UL pointing downstream, zig-zag strip location is marked, θ=30° h/C=0.28%, Re=160,000, α=18°. (a) baseline; (b) Cμ=4%

1. Steady blowing from a leading edge slot pointing in the direction of streaming

At $\alpha=18^o$ and Re=1.6*10^5 the baseline flow ($C_\mu=0$) separates near the slot but reattaches briefly just upstream of the juncture with the main element before separating completely near the first trip strip (Fig. 18a). The naturally separated flow sets up a mixing layer that is parallel to the free stream. Blowing at $C_\mu<1\%$ has no observable effect on reattachment but once a threshold value of blowing is surpassed (somewhere around $C_\mu=2.5\%$ depending on the trip strip used) the flow reattaches up to the mid chord of the airfoil (x/c=0.5). At this point however, the leading edge bubble becomes often much longer and the upstream flow passes above the second zigzag transition strip before reattaching to the surface. It seems that a minimum threshold level of C_μ is required to turn the flow around the leading edge and to overcome the strong adverse pressure gradient associated with the combination of incidence and curvature near the LE. Upon surpassing this threshold the flow reattaches to the mid chord location where the increasing thickness provides additional pressure gradient relief. Downstream of the maximum thickness location, the flow has to overcome an additional adverse pressure gradient due to the thinning of the airfoil near its TE. For this reason doubling the C_μ had no effect on the lift and on the location of separation, that remained pegged at the mid chord point. A major difference in the separation location occurred at $C_\mu\approx10\%$ where the flow remained attached over 75% of the chord (not shown).

Steady blowing at zero incidence from a slot located on the upper surface at θ=30° pointing downstream does not have the same detrimental effect on lift as blowing from the TE did at low levels of C_μ [14]. This is because the slot is so far upstream of the separation location that the locally added boundary layer displacement near the LE is not affecting separation at the TE and thus the ensuing lift. For large α, however weak blowing enhances separation that occurs near the blowing slot whenever U_J is smaller than the local free stream velocity. This is best observed by examining the mean flow recorded by averaging 250 PIV records obtained for each flow condition and subtracting from them the ensemble averaged record of the baseline (Fig. 19).

At C_μ=0.3% the weak jet displaces the fluid downstream generating a velocity deficit region that is most obvious above the trip strip (Fig. 19a). This resembles the effect observed near the TE where weak blowing created negative lift. The velocity deficit shown in this case is much stronger than the deficit observed near the TE because the boundary layer is thin and the local flow outside the boundary layer exceeds U_∞. Blowing at C_μ=1.8% (Fig. 19b) displaces the flow upstream of the slot slowing the flow near the surface and it also creates a bubble downstream of the slot that reattaches at or beyond the trip strip. The bubble displaced the exterior streamlines accelerating the flow outside it, effectively thickening the LE, and adding slightly to the lift at all angles of incidence (Fig. 20).

The variation of lift with increasing incidence is plotted in Fig. 20 for Re=2.5*10^5. The baseline case yields $C_{Lmax}\approx 1.1$ independent of Re but the incidence angle at which the airfoil stalls at the lower Re is also lower. There is a slight increase in C_{Lmax} when C_μ=2.3% but the airfoil stalls more gently when blowing is applied. The lift and drag results obtained for $\alpha>20^o$ are tainted by wind tunnel wall interference that becomes substantial particularly for the higher momentum coefficients investigated. The separation location on the upper surface of the airfoil moves upstream from its 90% chord location at $\alpha\approx 20^o$ to the mid chord prior to complete stall. Blowing at C_μ=4% could not dislodge the separation location from the mid chord region as seen in Fig. 18 for a somewhat lower Re. However, the difference in C_D between these two cases (C_μ=0 & C_μ=4%) measured at $\alpha=14^o$ exceeds the input of C_μ. Increasing C_μ to 9% doubles the maximum lift generated at $\alpha=16^o$ by pushing the separation location past the mid chord point towards the trailing edge region and reduces the drag by $\Delta C_D=0.155$ thus significantly exceeding the input level of $C_\mu=0.091$. When the same C_μ input was introduced at lower incidence levels the benefits were

much lower (Fig. 20) and only ½ of the jet momentum was recovered as thrust. Thus steady blowing from the LE region is only beneficial when it can overcome separation over large portions of the upper surface.

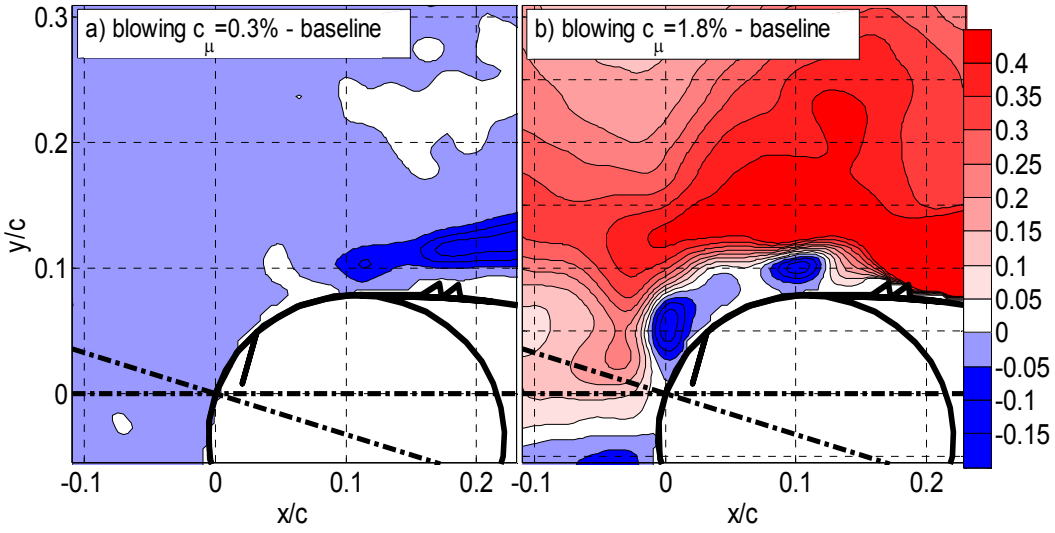

Fig. 19 Difference contours between blowing and baseline flow for slot located at θ=30°, h/C=0.28%, Re=160,000 & α=18°. A zigzag trip strip was used.

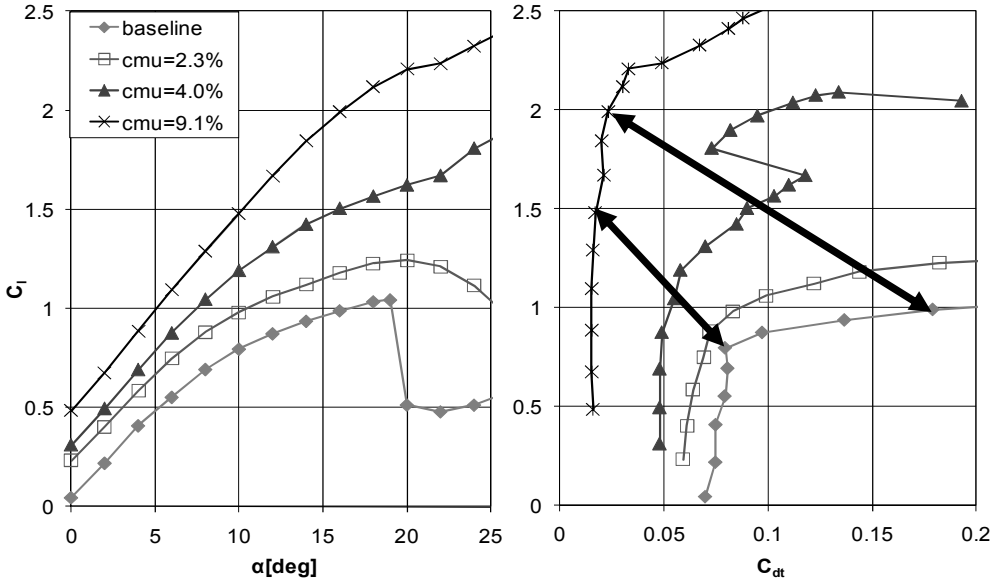

Fig. 20 Effect of C_μ on C_L and C_D, Re=250,000, LE actuation at θ=30°, h/C=0.28%, zigzag

Changing the tripping device affected not only the baseline performance of the airfoil but also the incremental increase in lift, ΔC_L, at prescribed levels of C_μ. The differences were of the order of 10%, suggesting an interaction between the tripping device and the blowing as seen in Fig. 21. Smoke emanating from the slot indicates that at C_μ=0.3% the jet does not manage to attach the flow thus marking the separated mixing layer that is susceptible to Kelvin-Helmholtz instability and rolls up into discrete eddies (Fig. 21a). The strong reflection of light marks the location of the zigzag strip. The filament of smoke corresponding to C_μ=1.8% marks the boundary of a bubble that starts laminar before undergoing transition that ultimately results in reattachment of the flow over the trip strip. Increasing the C_μ to 9.1% causes early transition to turbulence upstream of the trip strip. Consequently the size, shape and location of the trip strip affects the C_μ that causes flow reattachment to the surface.

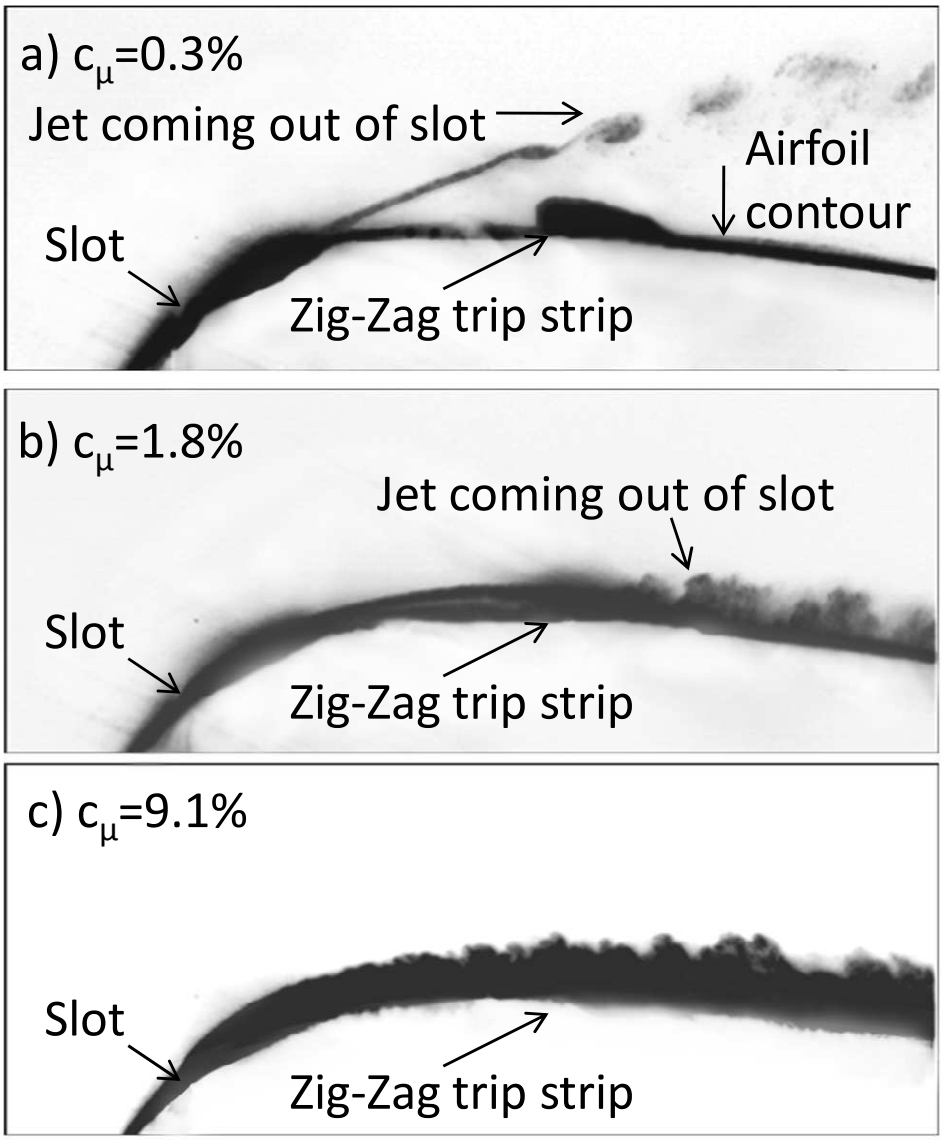

Fig. 21 Flow visualization showing the interaction between the jet and the trip strip at α=18°, Re=160,000, actuation at θ=30°, h/C=0.28%.

By changing the azimuth of the slot, θ, one also changes the distance between the slot and the trip-strip and it appears that this interaction is significant (Fig. 22). The jet emanating from θ=30° at C_μ=1.8% and high α, has sufficient distance to the trip-strip to undergo transition and reattach as turbulent flow. The same jet emanating from θ≥45° passes above the trip-strip without reattaching to the downstream surface. It thus has a weakly detrimental effect on the flow generated under these conditions. As a result the airfoil stalls somewhat earlier and generates less lift. (Fig. 22).

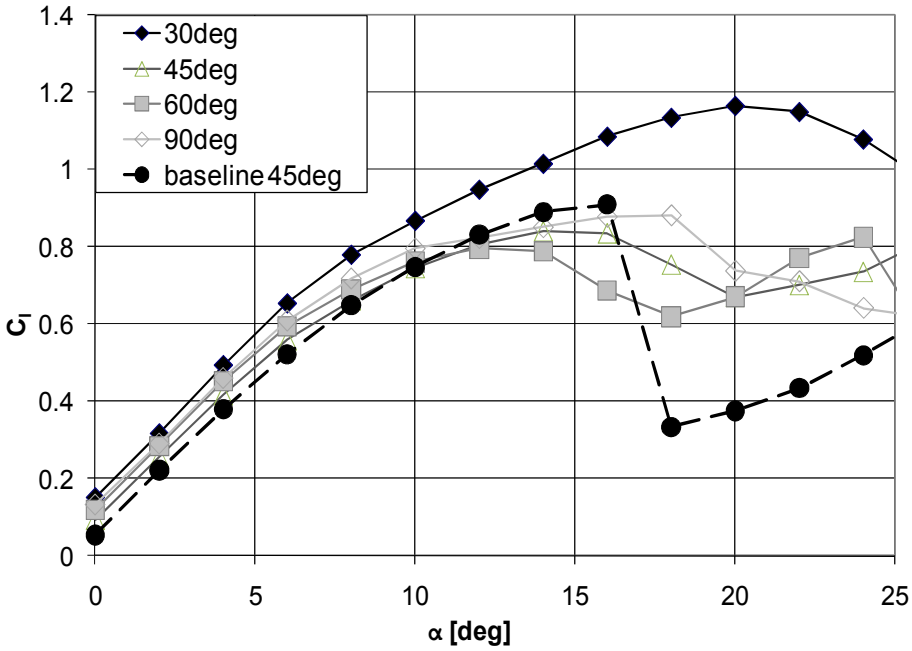

Fig. 22 Effect of θ on C_L at Re=250,000, LE actuation h/C=0.28%, C_μ=1.8%

J. Steady suction from a leading edge

The main purpose of locating AFC near the leading edge is to affect conditions created prior to stall, thus the dependence of the airfoil characteristics on incidence are discussed. The presence of the slot at large values of α affects the baseline conditions as discussed above. One should be reminded that the mere presence of the slot especially at large values of α, its location, orientation and width, affect C_{Lmax} and α_{stall} of the airfoil, so the relevant baseline data is presented as reference in the figures considered.

When suction was applied at a prescribed coefficient (e.g. C_Q=0.5%) the location of the slot had a dominant effect on lift and drag overshadowing every other variable. When the slot was located at $\theta=30^o$ the maximum lift increased to a mere $C_{Lmax}=1.17$ but for $\theta=90^o$ the airfoil did not stall at $\alpha=25^o$ yielding a $C_{Lmax}>1.8$ for the same C_Q used (Fig. 23a). Suction from the farther locations enables the flow to turn around the leading edge without separating whereas the same suction from $\theta=30^o$ does not have the necessary control authority. The lack of directivity of the suction slot prevents the flow from turning around the circular cylinder that forms the LE whenever the slot is too close to the LE as the fluid moving toward the slot decelerates the main stream. Changing the slot orientation did not affect the results in any substantial manner. Therefore, neither the lift nor the drag reduction due to suction from a slot that scoops the incoming flow by pointing upstream, are presented (the results are almost identical to those shown in Fig. 23).

The effect of slot location on the drag at a given high C_L and a prescribed C_Q is also significant. For example at $C_L \approx 1.17$ the drag corresponding to $\theta=30^o$ was $C_D=0.18$. It was reduced to $C_D=0.08$ by moving the slot to $\theta=90^o$ without changing the C_Q but changing α in order to maintain a constant C_L (Fig. 23b). The effect on drag between $\theta=30^o$ and $\theta=90^o$ is substantial at all angles of incidence as it exceeds ΔC_{Dt} of 0.03 even at small angles α. It appears that suction lowers the pressure over the LE and by doing so it thins the boundary layer that turns around the LE thus also delaying separation at the blunt TE. In short, suction has a beneficial effect associated with viscous and turbulent losses and it does not just simply modify the potential flow. Ineffective suction through a slot located at $\theta=30^o$ increases the drag above the baseline configuration when most of the flow on the ellipse is still attached at $\alpha<10^o$. This $\Delta C_{Dt} \approx 2C_Q$.

Comparing the pressure distributions measured at large incidence angles when identical suction was applied at $\theta=30^o$ & 90^o reveals the need to accelerate the flow around the entire circular leading edge. At $\alpha=20^o$, the minimum C_p corresponding to $\theta=90^o$ is much lower than the one corresponding to $\theta=30^o$ resulting in attached flow that extends over 80% of the chord (see inset to Fig. 23c), whereas the Cp corresponding to $\theta=30^o$ suggests that the flow separated around x/c=60%. At $\alpha=22^o$, the slot located at $\theta=30^o$ entirely failed to turn the flow around the leading edge resulting in LE stall. (Fig. 23a).

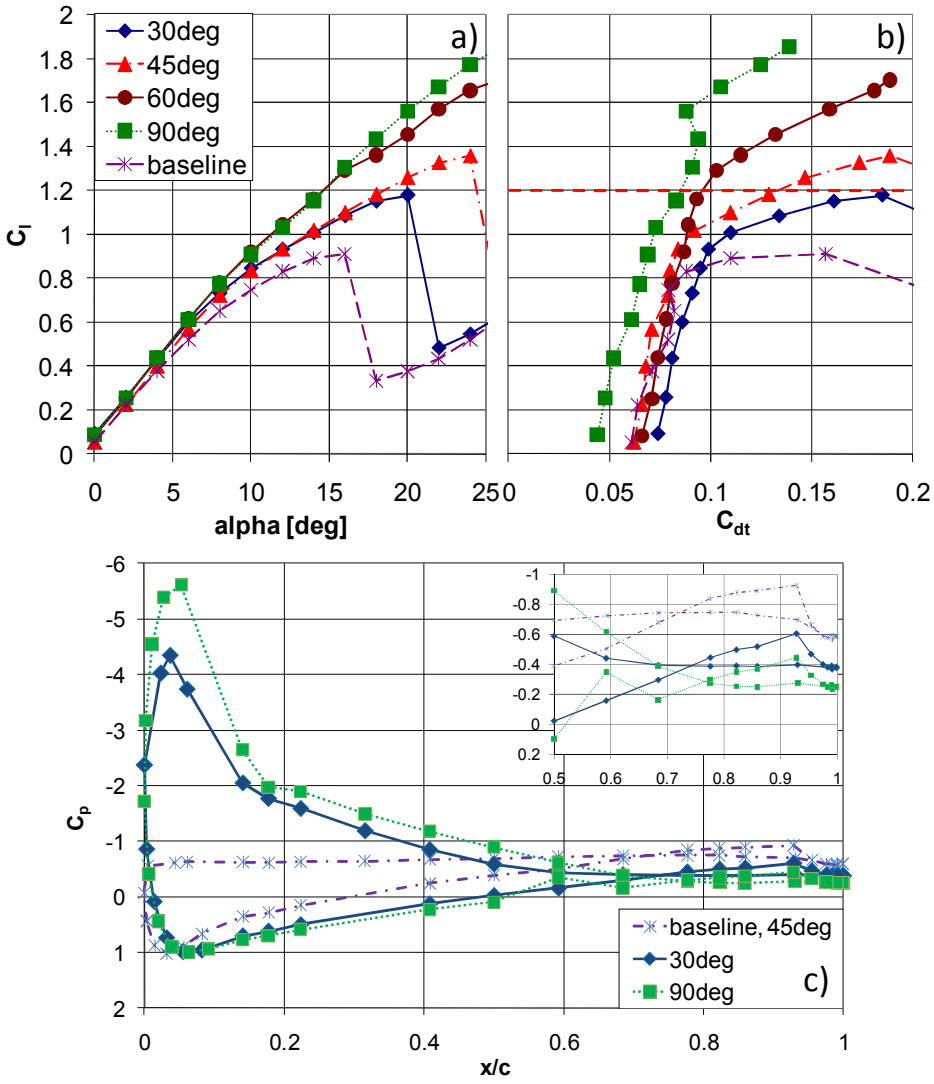

Fig. 23 Effect of slot location on: (a) lift; (b) drag; (c) pressure distribution generated by suction. Slot pointing downstream Re =2.5*10^5, C_Q=0.5%; h/C=0.28%

Another observation accentuating the significance of the slot location is the early saturation of the flow at a given θ with increasing C_Q. When the slot was located at a wrong position (e.g. $\theta=30^o$), suction was unable to increase C_L regardless of the level of suction applied. This is because the suction slot brought in fluid from the upper surface downstream of it, rather than pulling it from the region between the stagnation location and the slot, therefore having little or no effect on the separation from the upper surface.

Reversing the slot orientation to the upstream direction but maintaining its location and width did not alter the incremental results shown in Fig. 23 when suction was applied. Suction also reduced the measured C_{Dt} by approximately $2C_Q$ as it did before. These results suggest that the incremental improvements resulting from suction are not affected by slot orientation near the leading edge. Slot location however may even be more important than an increase in C_Q.

IV. CONCLUSION

Baseline and active flow control cases for the ellipse were investigated using CFD with the Spalart-Allmaras turbulence model. Overall, it was found that the time averaged lift coefficients predicted by the code were similar to the experimental results. Also, the predicted pressure coefficient along the surface of the ellipse was similar to lab

results for the ellipse and the ellipse with the cusp. The negative lift slope curve for the ellipse with the cusp was also predicted well by the code. The results for trailing edge blowing at zero angle of attack were similar to lab results. The maximum negative value of C_L for blowing downstream and the shape of the C_L vs. C_μ curve were predicted well. For trailing edge blowing and suction it was found that the value of C_L was slightly underestimated by the code for the ellipse, and overestimated for the ellipse with the cusp.

Additionally, Actuation from the leading edge was investigated. Generally, the effectiveness of Blowing is improved when it is applied with the narrowest possible slot location upstream of the separation location while suction is most effective downstream of the natural separation location with a wide slot. For large α, weak blowing from the leading edge enhances separation that occurs near the blowing slot whenever U_J is smaller than the local free stream velocity. This resembles the effect observed near the TE at $\alpha=0^o$ where weak blowing created negative lift.

Changing the tripping device affected not only the baseline performance of the airfoil but also the incremental increase in lift, ΔC_L, at prescribed levels of C_μ. The differences were of the order of 10%, suggesting an interaction between the tripping device and the blowing. Consequently the size, shape and location of the trip strip affects the C_μ that causes flow reattachment to the surface.

V. ACKNOWLEDGMENTS

The project is sponsored by NASA under contract # NNX07AB73A and it is carried out in collaboration with the "Fluid Dynamics Branch" headed by A. Washburn.

VI. BIBLIOGRAPHY

[1] Maskell, E. G., Flow separation in three-dimensions. Report No. Aero 2565, Royal Aircraft Establishment, Farnborough, 1955

[2] Chang, P. K., "Control of flow separation: Energy conservation, operational efficiency, and safety", Research supported by the U.S. Navy; Washington, D.C., Hemisphere Publishing Corp.; New York, McGraw-Hill Book Co., 1976. 537 p.

[3] Telionis, D.P., Unsteady Boundary Layers Separated and Attached, *Journal of Fluids Engineering*, Vol. 101, No. 1, pp. 29-43, 1979

[4] Gad-el-Hak, M., and Bushnell, D.M., "Separation Control: Review," Journal of Fluids Engineering 113, pp.5-30, 1991

[5] Simpson, R.L., "Turbulent Boundary-Layer Separation", Annual Review of Fluid Mechanics, Vol. 21: 205 -232 (Volume publication date January 1989)

[6] Simpson, R.L., "Aspects of turbulent boundary-layer separation", Progress in Aerospace Sciences, Volume 32, Issue 5, October 1996, Pages 457-521, ISSN 0376-0421, DOI: 10.1016/0376-0421(95)00012-7.

[7] Bradshaw & Wong, Journal of Fluid Mechanics (1972), 52:1:113-135 Cambridge University Press, 1972, doi:10.1017/S002211207200299X

[8] Kim, J., Kline, S.J., Johnston, J.P., "Investigation of a Reattaching Turbulent Shear Layer: Flow Over a Backward-Facing Step" J. Fluids Eng. -- September 1980 -- Volume 102, Issue 3, 302 (7 pages), doi:10.1115/1.3240686

[9] Prandtl, L. "The Generation of Vortices in Fluids of Small Viscosity", *Journal of the Royal Aeronautical Society*, Vol. 31, 1927, p. 735.

[10] Malik, MR and Bushnell, DM, "Role of Computational Fluid Dynamics and Wind Tunnels in Aeronautics R&D", NASA Technical Paper, 2010

[11] Englar R., in *Applications of Circulation Control Technology, Progress in Astronautics and Aeronautics,* Joslin R.D and Jones G.S. (eds.), Vol. 214, 2006.

[12] Poisson-Quinton, Ph., "Recherches Theoriques et Experimentales Sur le Controle de Couche Limites", *VII International Congress of Applied Mechanics,* London, 1948

[13] Chen, C., Zakharin, B., and Wygnanski, I., "On the Parameters Governing Fluidic Control of Separation and Circulation," AIAA-2008-629, 2008.

[14] Chen, C., Seele, R., and Wygnanski, I., "On the Comparative Effectiveness of Steady Blowing and Suction Used for Separation and Circulation Control on an Elliptical Airfoil," AIAA-2010-4715, 2010.

[15] Hoerner, S. F., "Fluid-Dynamic Lift," Hoerner Fluid Dynamics, Bakersfield, 1985.

[16] White, F. M., "Viscous Fluid Flow," McGraw-Hill Inc., New York, 1974.

[17] Bachelor, G. K., "An Introduction to Fluid Dynamics," Cambridge Univ. Press, Cambridge, England, 1967.
[18] Baldwin, B. S., Lomax, H., "Thin Layer Approximation and Algebraic Model for Separated Turbulent Flows," AIAA-78-257, 1978.
[19] Spalart, P. R., and Allmaras, S. R., "A One-Equation Turbulence Transport Model for High Reynolds Number Wall-Bounded Flows," NASA-TM-102847, 1990.
[20] Wilcox, D. C., "Turbulence Modeling for CFD," 2nd Edition, La Canada, California: DCW Industries, Inc., 1998.
[21] Menter, F. R., "Improved Two-Equation k - ω Turbulence Models for Aerodynamics Flows," NASA-TM-103975, 1992.
[22] Nishri, B. and Wygnanski, I., "Effects of Periodic Excitation on Turbulent Flow Separation from a Flap," *AIAA Journal*, Vol. 36, No. 4, 1998.
[23] Bartels, R. E., Rumsey, C. L. and Biedron, R. T., "CFL3D Version 6.4 – General Usage and Aeroelastic Analysis," NASA-TM-2006-214301, 2006.
[24] Chan, W. M., "The Overgrid Interface for Computational Simulations on Overset Grids," AIAA-2002-3188, 2002.
[25] Biedron, R. T. and Rumsey, C. L., "CFL3D User's Manual Version 5.0," NASA-TM-1998-208444, 1998.